energies

MDPI

Article

The Underground Coal Gasification Process in Laboratory Conditions: An Experimental Study

Marek Laciak *, Milan Durdán, Ján Kačur and Patrik Flegner

Faculty BERG, Institute of Control and Informatization of Production Processes, Technical University of Košice, Němcovej 3, 04200 Košice, Slovakia

* Correspondence: marek.laciak@tuke.sk; Tel.: +421-55-602-5175

Abstract: The underground coal gasification (UCG) process represents a modern and effective coal mining technology that enables coal energy extraction through thermic decomposition. The coal is transformed into syngas by oxidizers (e.g., air, technical oxygen, or water steam) and is injected into a georeactor. The produced syngas is exhausted on the surface, where it is transformed into the desired form of energy. This paper presents an experimental study of two experiments performed in ex-situ reactors. The paper describes the equipment for the UCG process, the physical models of the coal seam, and the analysis of coal. The obtained results from the experiments are presented as the behavior of the temperatures in the coal during the experiment, the syngas composition, and its calorific value. The material balance and effective gasification time of the UCG process were also identified for the individual experiments. The aim was to evaluate the impact of the coal seam model on the gasification process efficiency. Calculating the material balance during the gasification appears to be an effective tool for assessing leaks in the reactor while measuring the flow and concentration of the oxidizers and produced gas. The material balance data are make it possible to propose methods for controlling the input oxidizers. To increase the efficiency of the gasification in an ex-situ reactor, it is necessary to ensure the impermeable or poorly permeable surrounding layers of the coal seam.

Keywords: underground coal gasification; ex-situ reactor; syngas; experiment; material balance; efficiency

Citation: Laciak, M.; Durdán, M.; Kačur, J.; Flegner, P. The Underground Coal Gasification Process in Laboratory Conditions: An Experimental Study. *Energies* **2023**, *16*, 3266. https://doi.org/10.3390/en16073266

Academic Editor: Pavel A. Strizhak

Received: 14 March 2023
Revised: 30 March 2023
Accepted: 4 April 2023
Published: 5 April 2023

1. Introduction

Underground coal gasification (i.e., UCG) is a technique used for extracting coal energy through the conversion of coal into combustible gas primarily composed of hydrogen, methane, and carbon monoxide. The processes, such as drying, pyrolysis, gasification, and combustion, occur during this procedure. In addition, liquid tar products are also obtained, depending on the process conditions. UCG research is still a current topic. Since the realization of UCG trials is costly and complex, mathematical and experimental models are essential for UCG studies to predict the effects of various physical and operating parameters on the process performance. Some experimental studies based on a model experiment were realized to improve this process. For example, the impact of the oxygen–steam gasification, pure oxygen gasification, and moving-point gasification methods on the gas quality was tested using a model experiment [1]. The results showed that it was possible to effectively improve the changes in the coal seams cavity or the roof inbreak effects on the gas quality using moving-point gasification. The concepts, assumptions, and limitations of the packed bed models, the channel model, and the coal slab model were also experimentally modeled [2]. The results of these models demonstrated the applicability of the packed bed models for use in highly permeable porous media only, the suitability of a permeable channel between the injection and the production holes in the channels models, and the successful demonstration of the drying and devolatilization behavior of large coal particles in the coal slab models. An ex-situ surface reactor was constructed to assess the feasibility of applying underground hard coal gasification in hydrogen-rich gas

production [3]. The steam and oxygen were supplied to the reaction zone separately in alternate stages for the experiments realized in this reactor. This approach increased the concentration and the amounts of hydrogen in the product gas during the steam gasification stage. A lab-scale hydrogen-oriented experiment in an ex-situ reactor for the Turkish lignite gasification process was also performed [4]. Subsequently, these experimental data were used for a two-dimensional UCG computational fluid dynamic (i.e., CFD) model proposal. The proposed model visualized the distribution of the chemical species and reaction zones inside the reactor. In another study, gas chromatography–mass spectrometry was used to analyze the properties of the tar created during gasification in an experimental reactor [5]. The results showed the differences in the tar behaviors from the reaction zone and outlet, e.g., a smaller percentage of the high boiling point content and a higher percentage of H for the tar from the outlet. The methane-oriented UCG process was realized in a large-scale laboratory experimental reactor [6]. Two coal types, i.e., semi-anthracite and hard coal stored in this reactor, were used in the oxygen and steam-blown experiments. The mathematical and experimental models are essential for UCG studies to predict the effect of the various physical and operating parameters on the process performance since the realization of the UCG trials is costly and complex. An increase in the formed CH_4 and H_2 and a decrease in the CO_2 concentration were recorded at the water injection site. The study described in [7] discussed the application of a coaxial UCG system with a horizontal hole during the UCG experiments in the experimental reactor. The experiments used two types of coal and oxygen-enriched air. The results showed that the coal quality affecting the expansion area of the gasification moving an injection pipe was likely improve the quality of the product gas, and the calorific value of the product gas was improved corresponding to an increase in the oxygen supply. Coal specimens of different ranks were used during the experiments in an ex-situ reactor to characterize the inorganic constitutions generated at the various operating conditions [8]. The experiments were realized at various gaseous oxidant ratios, pressures, and temperatures. The decreasing cationic elements and increasing concentrations of anionic species were caused by increasing the amount of water in the oxidants. In addition, the high-pressure experiments at a temperature of 750 °C significantly reduced the cationic element generation, while the anionic species production was high.

Numerical models are used as a tool for modeling processes and optimizing technologies. Due to this, the material balance calculations and energy balance calculations are an integral part of the information acquisition about the efficiency of the processes. The effects of the gasification agent ratio on the product gas composition and calorific value were researched during the UCG laboratory experiments under different oxygen concentrations [9]. In addition, the energy recovery rate and coal consumption were evaluated using an energy recovery evaluation method. This method was based on the carbon balance. The results showed a positive effect for increasing the oxygen concentration on the increasing calorific value of the produced gas. Furthermore, it was possible to determine an estimate of the coal consumption for the UCG experiments using the carbon balance method. The material balance equations were also used to propose combustible gas equivalents [10]. Stoichiometry and the material balance converted the generated gas product into a combustible gas equivalent. Subsequently, the gradient formula was used to obtain the trends in the equivalents. The results from this procedure were used to propose a dual-source extended short-term memory prediction model for predicting the UCG state. The regularities of the heat and mass balance changes in the faulting zones of thin coal seams were also researched [11]. This research analyzed the influence usage of the air and the oxygen-enriched blast. The mass balance proved to be a convenient tool for predicting the output parameters and indicators (i.e., quantitative and qualitative). A coupled seepage-thermodynamics-transport model was proposed to examine the impact of contaminants on groundwater [12]. This model was based on mass and energy conservation. The results showed that the contaminants' migration velocity depended on the heat, seepage, stress, physicochemical reactions, etc. The modified energy balance equation was used to simulate

the coal-burning process and create a thermal-mechanical numerical model [13]. This model was used to evaluate the ground subsidence caused by the worst-case scenario regarding the potential size of a formed cavity. The heat and mass balance was also used to study the UCG parameters and the rock mass of the stress-deformed state around the gas gasifiers [14]. The calculations showed a maximum length for the gasification pillar and recommendations for the use of the gasifiers' construction through drill-injected blast activators. Furthermore, non-linear partial and differential equations were used to describe the energy and mass balances for the coal and char [15]. The proposed model simulated the temperature profiles in the coal seam, mass and heat transport, and the chemical reactions during the gasification process. The calculation for the one-dimensional (1D) model was realized using the Galerkin finite element method and was compared to the finite difference method. The equations of the mass and energy balances were also used to describe the solid and gaseous phases in the UCG process [16]. In this study, the effect of the coal seam dimensions and the applied pressure gradient on the energy content of the output gas was demonstrated. The heat and mass balance calculations based on a mathematical model of the physical and chemical processes in the individual phases (i.e., solid, liquid, and gaseous phases) were used for the thin coal seams in the faulting zones of the coal basin [17].

The aim of this article is to provide an experimental study and assessment of the influence of the physical model of a coal seam on the efficiency of the gasification process using mathematical modeling tools. As mentioned above, the experimental modeling and numerical models (e.g., in the form of a material balance) were an integral part of the study and the modeling of the UCG process [18]; for example, a mathematical model that considered the effective modification of the active zones for heat transfer during the underground coal gasification [19]. As a result, two experiments were carried out in two different generators with different coal bed constructions to assess the gasification efficiency using the material balance and the effective gasification time. The efficiency of the material balance was evaluated regarding the minor environmental losses and converted the input components, such as coal, air, and oxygen, into heating gas and liquid products. Two types of the material balance were used for the assessment, namely the total material balance (i.e., the balance of the weights of the input and output components of gasification) and the elementary material balance (i.e., the balance of the elemental components that were dominant in the overall material balance).

2. Materials and Methods

The gasification efficiency of the selected coal models was examined using the experiments in the ex-situ reactors. These were evaluated using the material balance and the efficiency time of the UCG process.

2.1. Experiments

The two experiments for identifying the UCG process were realized in two laboratory reactors (Figure 1). The first reactor was in the shape of a multi-part steel container designated as G1, and the second with a removable top was designated as G2. The G1 reactor had the shape of a large steel container (5 m long, 1.5 m wide, and 0.5 m high), while on its upper side, there was an opening lid composed of several parts. The G2 generator had the shape of a truncated cylinder with a length of 3 m and allowed for the insertion of the steel tube probes. Tubular probes were used for the process analysis along the length of the generator, i.e., the gas concentration measurement, temperature, and pressure measurement. The G2 generator had a compact one-piece lid, which required an electric lifting device to move. Except for the used reactor, these experiments differed in the physical model of the coal seam.

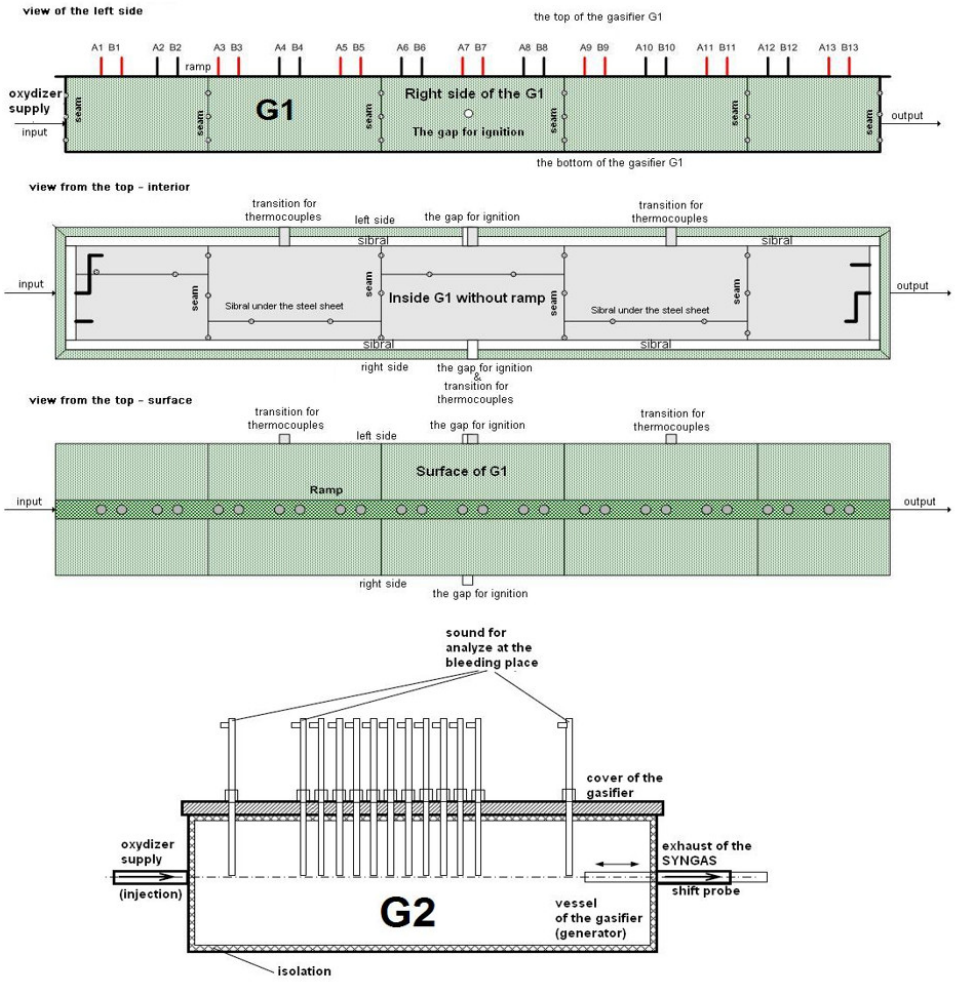

Figure 1. The scheme of the laboratory reactors G1 (**top**) and G2 (**bottom**).

2.1.1. The Analysis of the Coal

The coal composition obtained from a technical analysis of the coal sample at an accredited Slovak laboratory is shown in Table 1. In addition, the oxygen percentage was calculated.

Table 1. The analysis of the coal with the help of Slovak testing standards used by an accredited laboratory (Abbreviations: *r*—received, *d*—dry, *daf*—dry ash-free, *a*—analytical, G—gravimetry, EA—elementary analysis with conductive heat detector, K—calorimetry, RFS—X-ray fluorescence spectrometry).

Parameter	Value	Uncertainty	Method	Standard
Total moisture W_t^r (%)	13.8	5	G	PN 16.3
Ash A^d (%)	12.0	2	G	PN 16.4
Volatile V^{daf} (%)	46.4	4	G	PN 16.2
Carbon C^{daf} (%)	76.4	2	EA	PN 16.7
Hydrogen H^{daf} (%)	5.60	3	EA	PN 16.7
Nitrogen N^{daf} (%)	1.34	10	EA	PN 16.7
Calorific value Q_i^{daf} (MJ/kg)	29.9	2	K	PN 16.2
Calorific value Q_i^d (MJ/kg)	26.3	2	K	PN 16.1
Calorific value Q_i^r (MJ/kg)	22.3	2	K	PN 16.1
Ash A^r (%)	10.3	2	G	PN 16.4
Carbon C^r (%)	58.0	2	EA	PN 16.7
Hydrogen H^r (%)	4.25	5	EA	PN 16.7
Nitrogen N^r (%)	1.02	10	EA	PN 16.7

Table 1. *Cont.*

Parameter	Value	Uncertainty	Method	Standard
CaO (%)	2.02	5	RFS	PN 3.1
MgO (%)	0.38	10	RFS	PN 3.1
SiO_2 (%)	4.10	5	RFS	PN 3.1
Al_2O_3 (%)	2.59	5	RFS	PN 3.1
Fe_2O_3 (%)	1.09	10	RFS	PN 3.1
Na_2O (%)	<0.2		RFS	PN 3.1
P_2O_5 (%)	<0.02		RFS	PN 3.1
TiO_2 (%)	0.08	10	RFS	PN 3.1
K_2O (%)	0.07	10	RFS	PN 3.1
Volatiles V^r (%)	35.2	4	G	PN 16.2
Analytical moisture W^a (%)	9.52	5	G	PN 16.3
Total sulphur S_t^r (%)	0.71	15	G	PN 16.5
Sulphate sulphur S_s^r (%)	<0.01	20	G	PN 16.5
Sulphite sulphur S_p^r (%)	0.29	20	G	PN 16.5
Organic sulphur S_o^r (%)	0.42	20	G	PN 16.5
Oxygen O^{daf} (%)	15.95			
Oxygen O^d (%)	10.25			

2.1.2. The Physical Model of the Coal Seam

The scheme of the cross-section for the physical model of the coal seam for the first experiment (i.e., realized in the first reactor) is shown in Figure 2. The cross-section for the second experiment (i.e., realized in the second reactor) is shown in Figure 3. The weight of the used coal for the first experiment was 576 kg and 201 kg in the second.

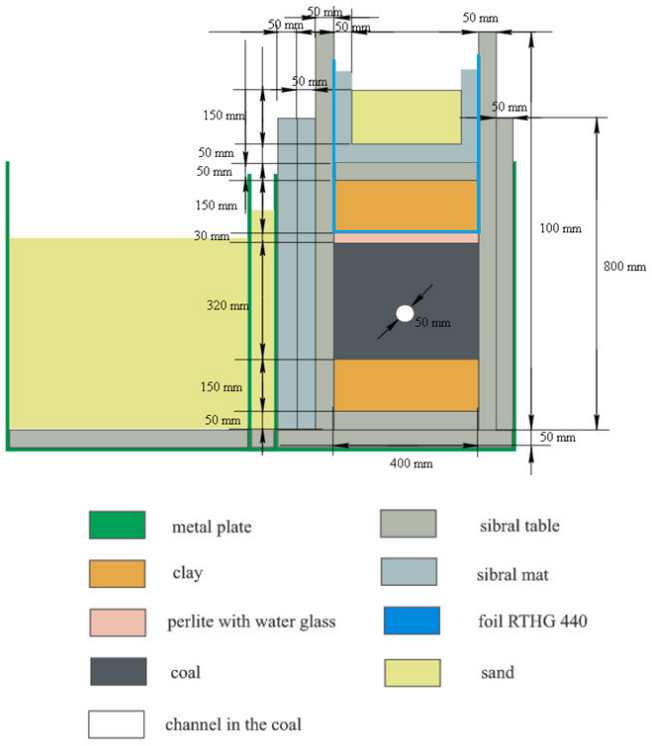

Figure 2. The scheme of the cross-section for the physical model of the coal seam for the first experiment.

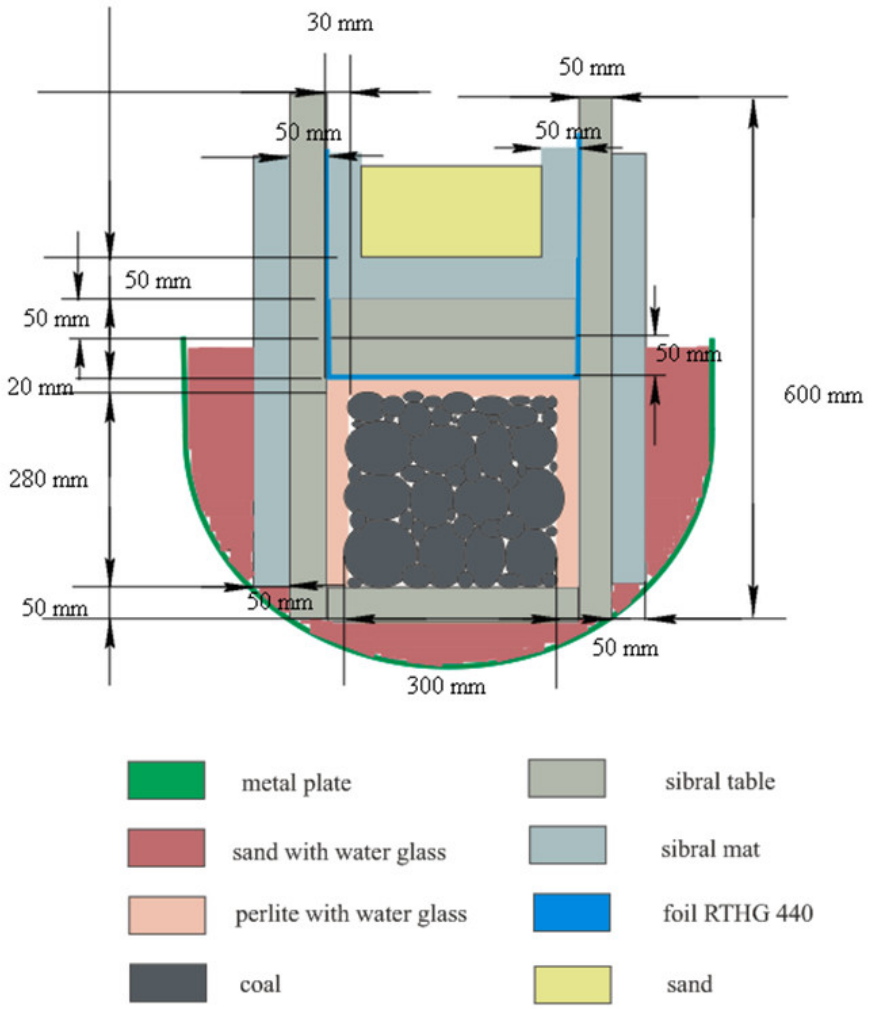

Figure 3. The scheme of the cross-section for the physical model of the coal seam for the second experiment.

2.1.3. Measurement of the Temperature in Ex-Situ Reactor

The distribution of the thermocouples in the G1 reactor is shown in Figure 4. There were seven thermocouples (1–7) in the gasification channel and ten thermocouples in the coal, of which five were on the left side of the gasifier inlet (8–12) and five were on the right side (13–17). Additional thermocouples were placed below and above the insulating layer of the sibral. There were a total of five cuts along the gasifier. In the insulating layer, there were eight thermocouples in each cross-section of the gasifier. Not all the insulating layers of the gasification device are shown in the figure [20,21].

The thermocouples were placed in the G2 reactor according to the diagram in Figure 5. The thermocouple T1 was placed at the ignition head's junction and the angular model's front face from the input side of the generator. There were eighteen thermocouples placed in the coal, of which nine thermocouples were in the longitudinal axis of the generator–central thermocouples (2–9), five on the left side of the generator from its entrance (10–14), and five on the right side (15–19). Additional thermocouples were placed below and above the insulating layer of the sibral. Similarly, in each section, the thermocouples were placed on the outer surface (twenty thermocouples) [22].

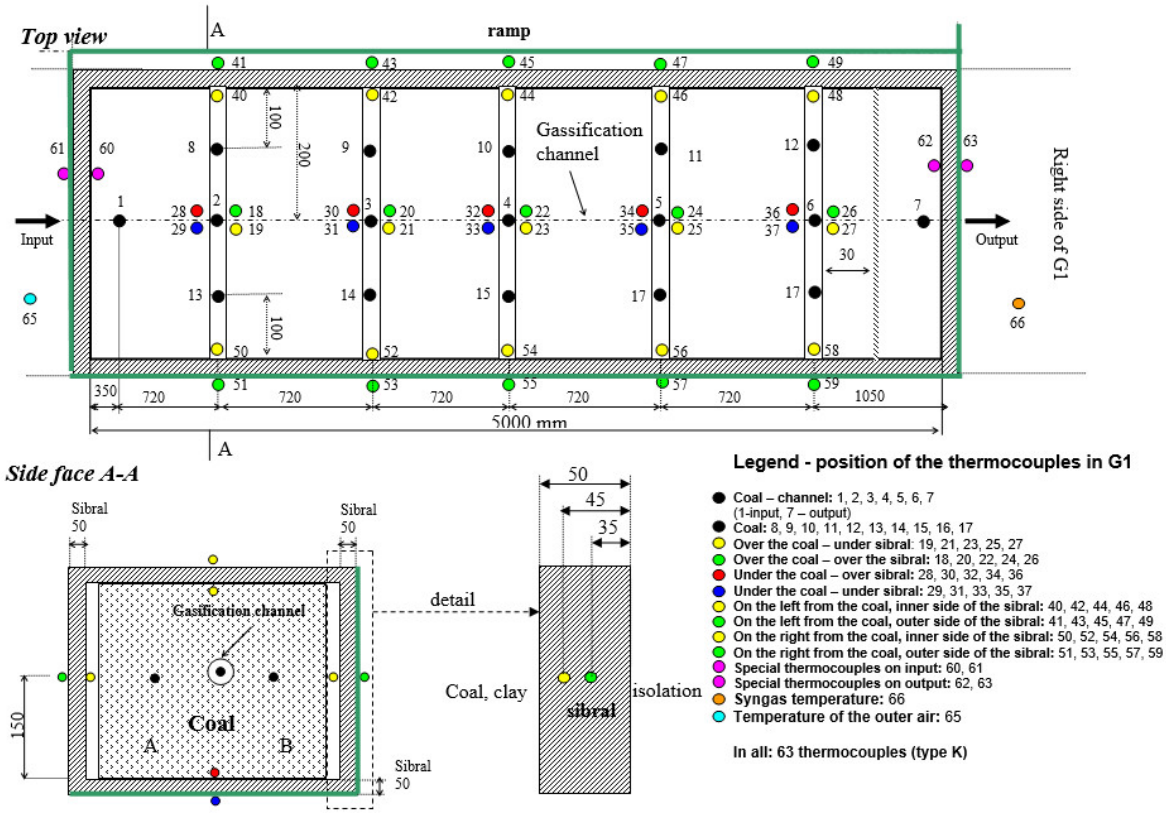

Figure 4. The scheme of the position of the thermocouples in the reactor for the first experiment.

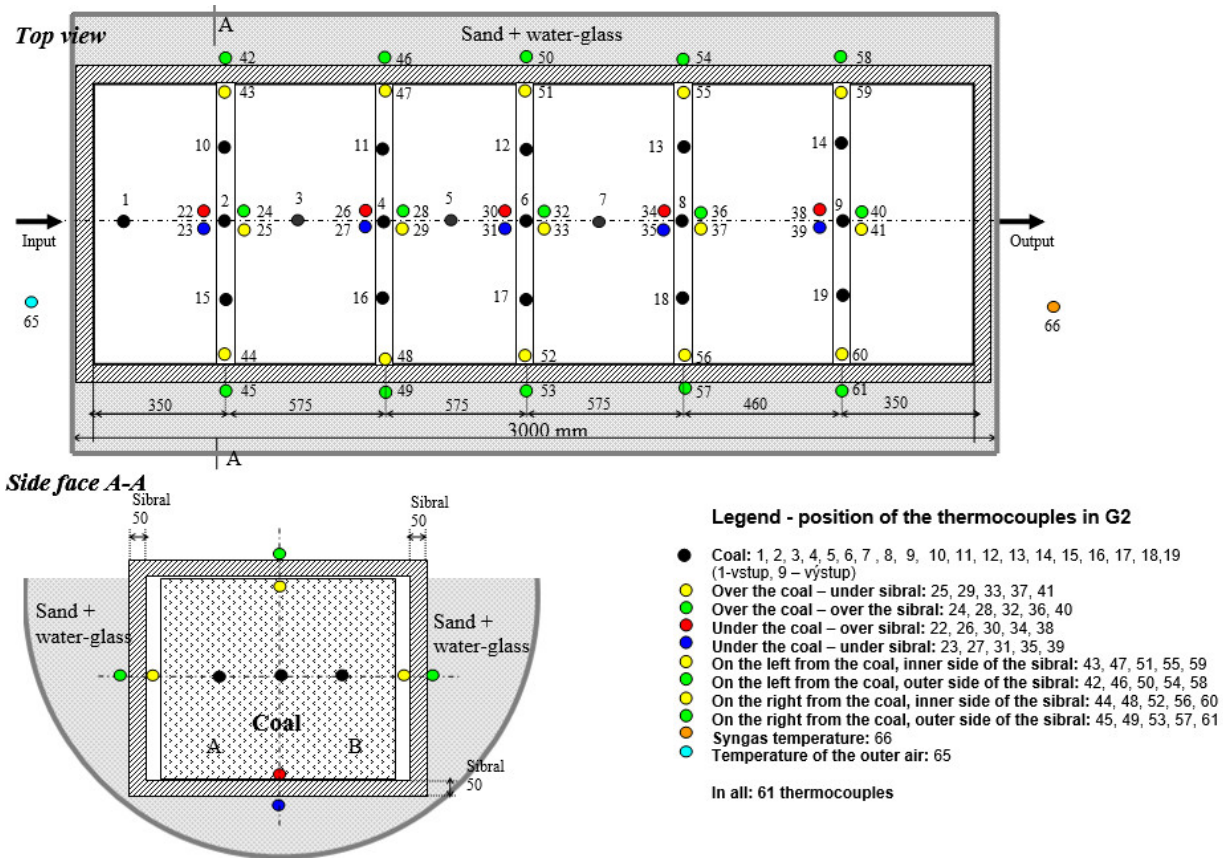

Figure 5. The scheme of the position of the thermocouples in the reactor for the second experiment.

In addition to the mentioned thermocouples located in the reactors, two were located outside in both experiments. The first thermocouple was used to measure the temperature of the surrounding air, and the second to measure the temperature of the syngas.

2.2. Material Balance Method

A material balance was derived from the principle of the mass conservation of the UCG process realized in the laboratory reactors. In this process, the input materials were the coal and the oxidizers (i.e., a mixture of air and oxygen). The output materials were the syngas, unburned coal, ash, and condensate (Figure 6). The total mass of the input materials must equal the total output mass.

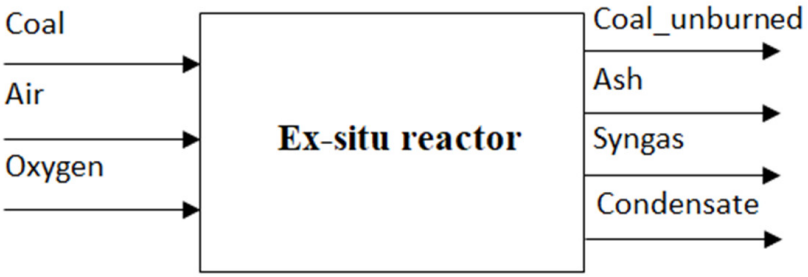

Figure 6. Scheme of the material balance in the ex-situ reactor.

A general mass balance of the UCG process is described by the following equation.

$$G_{coal} + G_{air} + G_{oxygen} = G_{coal,unburned} + G_{ash} + G_{gas} + G_{condensate}, \quad (1)$$

where G_{coal} is the mass of the coal, i.e., at the beginning of the process (kg); G_{air} is the mass of the used air (kg); G_{oxygen} is the mass of the used oxygen (kg); $G_{coal,unburned}$ is the mass of the unburned coal, i.e., at the end of the process (kg); G_{ash} is the mass of the ash (kg); G_{gas} is the mass of the syngas (kg); and $G_{condensate}$ is the mass of the condensate leaked during the process (kg).

In the UCG process, a higher temperature is needed to realize the chemical reactions and, subsequently, for the produced gas creation. The general mass balance can be rewritten using the conservation principle of the atoms as the elements. An atomic species balance assumes that the atomic species can neither be generated nor consumed in chemical reactions [23,24]. The atomic species balances for the considered elements of carbon C, hydrogen H, nitrogen N, oxygen O, and sulfur S have the following equations.

$$G_{coal,C} = G_{coal,unburned,C} + G_{gas,C} \quad (2)$$

$$G_{coal,H} = G_{coal,unburned,H} + G_{gas,H} + G_{condensate,H} \quad (3)$$

$$G_{coal,N} + G_{air,N} = G_{coal,unburned,N} + G_{gas,N}, \quad (4)$$

$$G_{coal,O} + G_{air,O} + G_{oxygen,O} = G_{coal,unburned,O} + G_{gas,O} + G_{condensate,O}, \quad (5)$$

$$G_{coal,S} = G_{coal,unburned,S} + G_{gas,S}, \quad (6)$$

where $G_{coal,C}$, $G_{coal,unburned,C}$, and $G_{gas,C}$ are the mass of the carbon in the coal and the produced gas (kg); $G_{coal,H}$, $G_{coal,unburned,H}$, $G_{gas,H}$, and $G_{condensate,H}$ are the mass of hydrogen in the coal, the produced gas, and the condensate (kg); $G_{coal,N}$, $G_{air,N}$, $G_{coal,unburned,N}$, and $G_{gas,N}$ are the mass of the nitrogen in the coal, air, and produced gas (kg); $G_{coal,O}$, $G_{air,O}$, $G_{oxygen,O}$, $G_{coal,unburned,O}$, $G_{gas,O}$, and $G_{condensate,O}$ are the mass of the oxygen in the coal, air,

oxygen, produced gas, and condensate (kg); and $G_{coal,S}$, $G_{coal,unburned,S}$, and $G_{gas,S}$ are the mass of the sulfur in the coal and produced gas (kg).

The individually measured chemical compounds (i.e., CO, CO_2, CH_4, H_2, N_2, O_2, and SO_2) were used to determine the chemical element mass in the produced gas. The C chemical element mass from the chemical compounds of the produced gas was determined according to

$$G_{gas,C} = V_{gas,CO} \cdot \rho_{CO} \cdot \frac{M_C}{M_{CO}} + V_{gas,CO_2} \cdot \rho_{CO_2} \cdot \frac{M_C}{M_{CO_2}} + V_{gas,CH_4} \cdot \rho_{CH_4} \cdot \frac{M_C}{M_{CH_4}}, \quad (7)$$

where $G_{gas,C}$ is the C chemical element mass in the produced gas (kg), $V_{gas,CO}$ is the CO chemical compound volume (m^3), V_{gas,CO_2} is the CO_2 chemical compound volume (m^3), V_{gas,CH_4} is the CH_4 chemical compound volume (m^3), ρ_{CO} is the CO chemical compound density ($kg \cdot m^{-3}$), ρ_{CO_2} is the CO_2 chemical compound density ($kg \cdot m^{-3}$), ρ_{CH_4} is the CH_4 chemical compound density ($kg \cdot m^{-3}$), M_{CO} is the CO chemical compound molar mass ($g \cdot mol^{-1}$), M_{CO_2} is the CO_2 chemical compound molar mass ($g \cdot mol^{-1}$), M_{CH_4} is the CH_4 chemical compound molar mass ($g \cdot mol^{-1}$), and M_C is the C chemical element molar mass ($g \cdot mol^{-1}$).

2.3. The Effective Gasification Time

The effective gasification time depends on the end use of the syngas and the conditions of the potential buyer of the syngas. For example, suppose the syngas will be used as fuel in thermal power plants, and the customer sets the condition of taking the syngas with a minimum calorific value of 3 MJ/Nm^3. In that case, this will also affect the effective gasification time.

Based on the effective gasification time, it is possible to calculate the percentage success of the experiment (i.e., $\%ESR$) from the point of view of the achieved calorific value (7).

$$\%ESR = \frac{time_{eff}}{time_{total}} \times 100, \quad (8)$$

where $time_{eff}$ is the effective gasification time of the UCG process and $time_{total}$ is the total time of the UCG process.

3. Results

The results from the two UCG process experiments are presented from the following points of view.

- The temperatures in the gasification channel
- The volume flow of the input oxidizers
- The syngas composition and calorific value
- The material balance
- The efficiency of the gasification process

3.1. The Temperature in the Gasification Channel

The course of the temperatures in the gasification channel during the first experiment is shown in Figure 7. Looking at the beginning of the gasification, one can see the increase in the temperature T1 above 1200 °C and its gradual decrease. Subsequently, an increase in the temperatures T2, T3, and T4, can be seen. Finally, the temperatures T5, T6, and T7 reached maximum values at the end of the gasification, up to 800 °C. The temperatures increased gradually as the gasification front moved along the length of the generator.

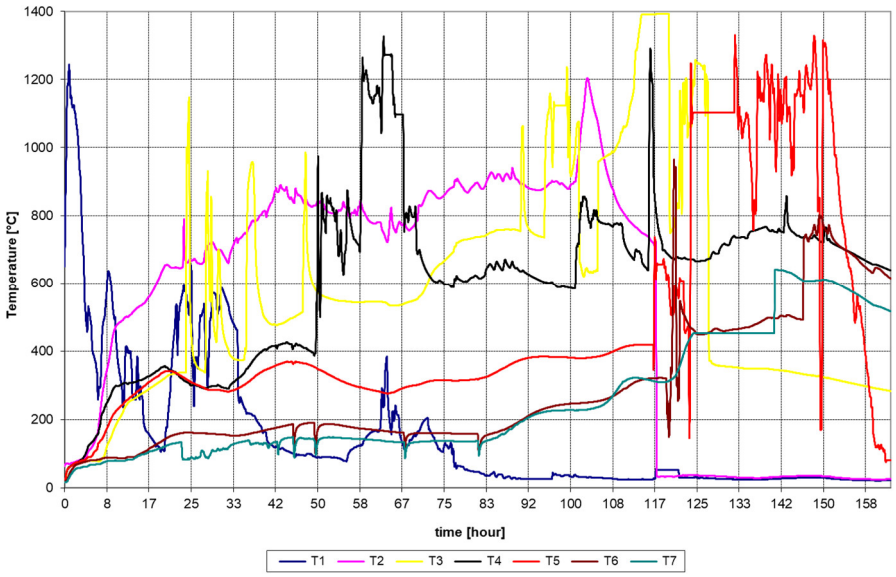

Figure 7. Temperature course in the gasification channel during the first experiment.

Figure 8 shows a 3D graph of the temperature trends in the channel. The x-axis is the thermocouple's position along the generator's length, the y-axis is represented by the time in minutes, and the z-axis is the temperature. The temperature is displayed in a color spectrum according to the legend. With this chosen presentation of the temperature course, it is logical that the gasification front moves diagonally from the lower left corner to the upper right corner.

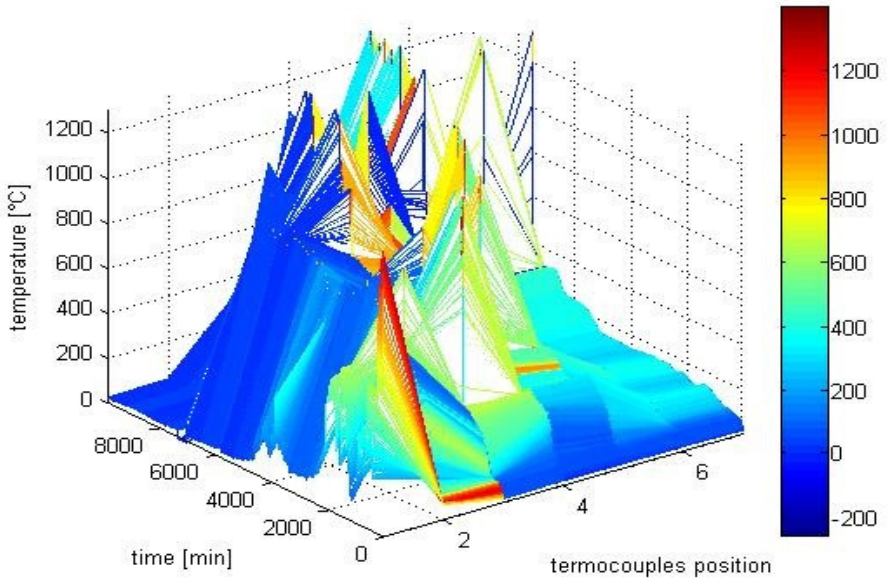

Figure 8. Time profile of the temperatures in the gasification channel along the length of the generator for the first experiment.

The course of the temperatures in the center of the coal seam during the gasification for the second experiment is shown in Figure 9. From the start of the gasification, a gradual increase in the temperatures can be seen along the length of the generator. First, the temperature T2 increased to a temperature of 1000 °C. When it decreased from this temperature, the temperature T3 already increased to a temperature of 1000 °C. Such a sequence of temperature increases along the length of the generator can be followed up to temperature T8, whose thermocouple was located before the end of the generator. It can be

stated that the temperatures increased gradually as the gasification front moved along the length of the generator. Figure 10 shows a 3D view of the temperatures along the length of the generator.

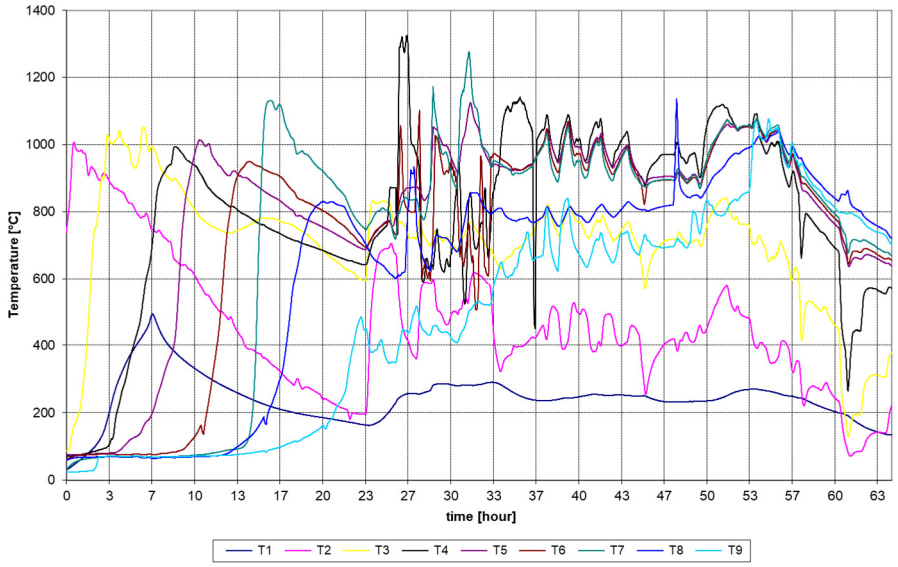

Figure 9. Temperature course in the gasification channel during the second experiment.

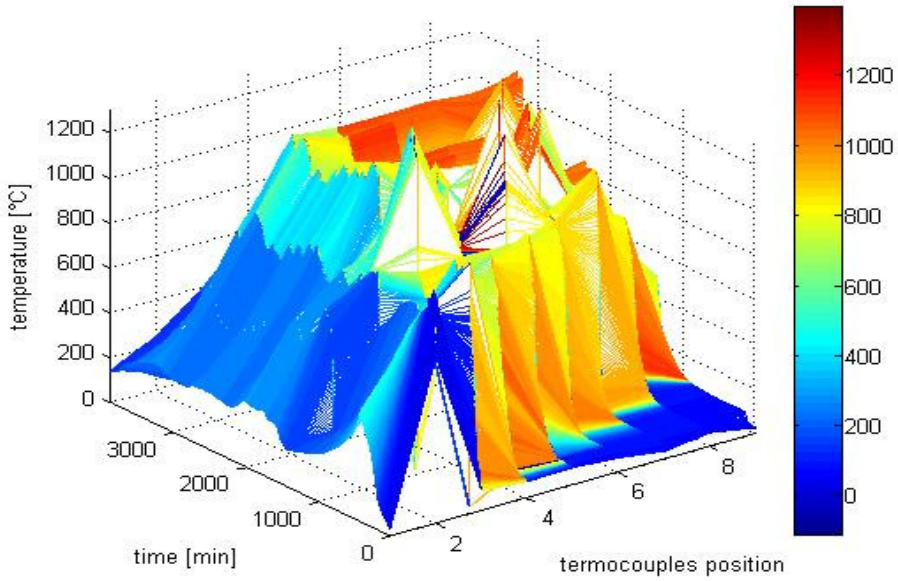

Figure 10. Time profile of the temperatures in the gasification channel along the length of the generator for the second experiment.

Figure 11 shows the maximum values of the temperatures in the gasification channel during both experiments. In the first experiment (Figure 11a), the temperature reached a value of 1000 °C in the second half of the experiment in contrast to the second experiment (Figure 11b), where the temperature fluctuated around the value of 1000 °C throughout most of the experiment.

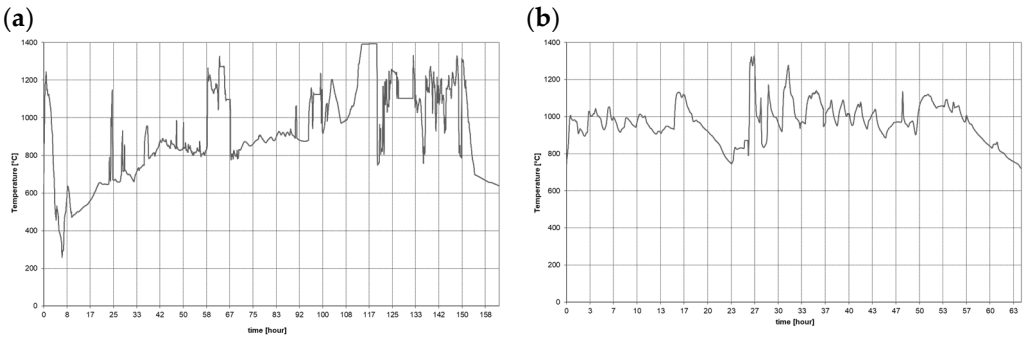

Figure 11. The maximal temperature course in the gasification channel (**a**) the first experiment (**b**) the second experiment.

3.2. Inputs Oxidizers

Figure 12 shows the course of the volume flows of the input oxidizers during the first experiment. The air, regarded as the primary oxidizer, was blown into the generator during the experiment from 0 to 40 Nm^3/h. The secondary oxidizer was technical oxygen, used in two time periods during the gasification. The first section was from 56 to 67 h, and the second was from 107 to 112 h of the experiment.

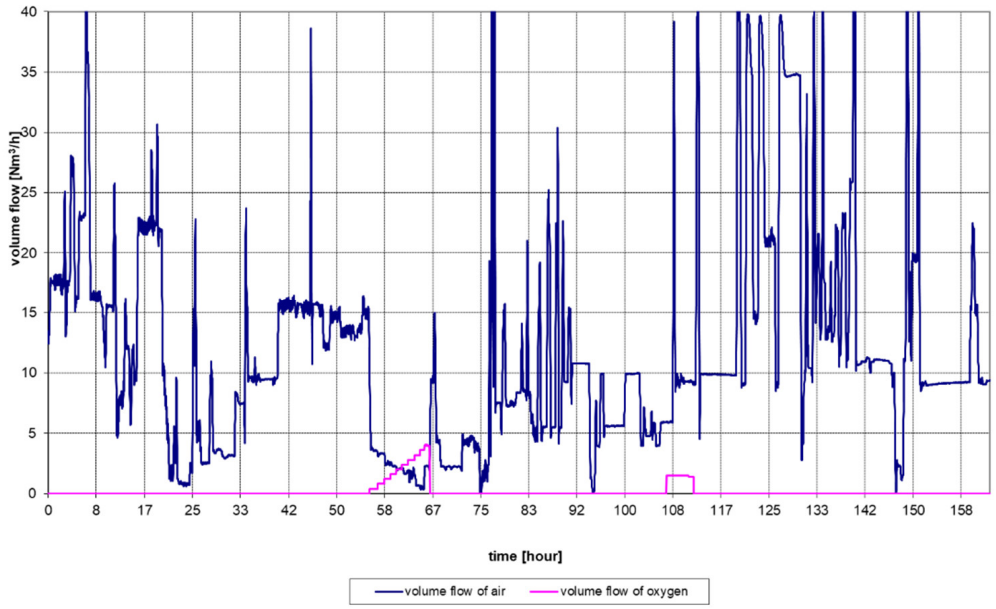

Figure 12. The volume flow of the oxidizers course during the first experiment.

Figure 13 shows the course of the volume flows of the input oxidizers for the second experiment. The air volume flow was almost consistent throughout the experiment between 0 and 15 Nm^3/h except at the end of the process, where increased to 20 to 35 Nm^3/h. With this short-term increase in the volume flow, an attempt was made to restart the gasification process, which failed (i.e., the reactor temperatures dropped and the calorific value was low). The technical oxygen was regarded as the secondary oxidizer used in the second half of the experiment at the interval from 0 to 4 Nm^3/h.

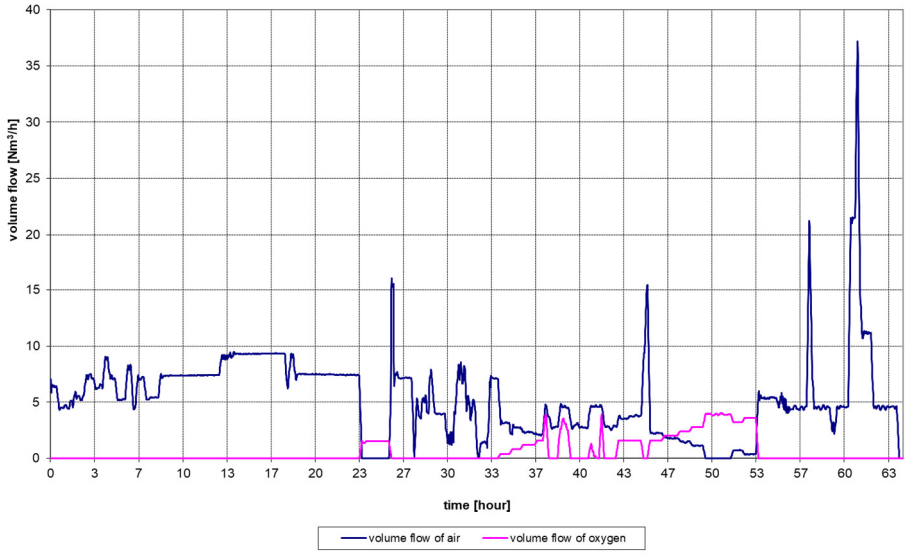

Figure 13. The volume flow of the oxidizers course during the second experiment.

3.3. The Syngas Composition and Calorific Value

Figure 14 shows the course of the syngas composition (i.e., CO_2, CO, CH_4, H_2) during the first experiment. The maximum concentration values of the individual components of the syngas were 50%. In two time periods, the gasification measured the highest concentrations of the heating components of the syngas, namely when using the oxidizer mixture of oxygen and air. The maximum temperature in the reactor in the first period was approximately 1310 °C (Figure 7), and the concentration of the heating components of the syngas were 49% CO and 36% H_2, respectively. In the second period, the temperature was approximately 1380 °C (Figure 7), the concentration was 49% CO and 33% H_2.

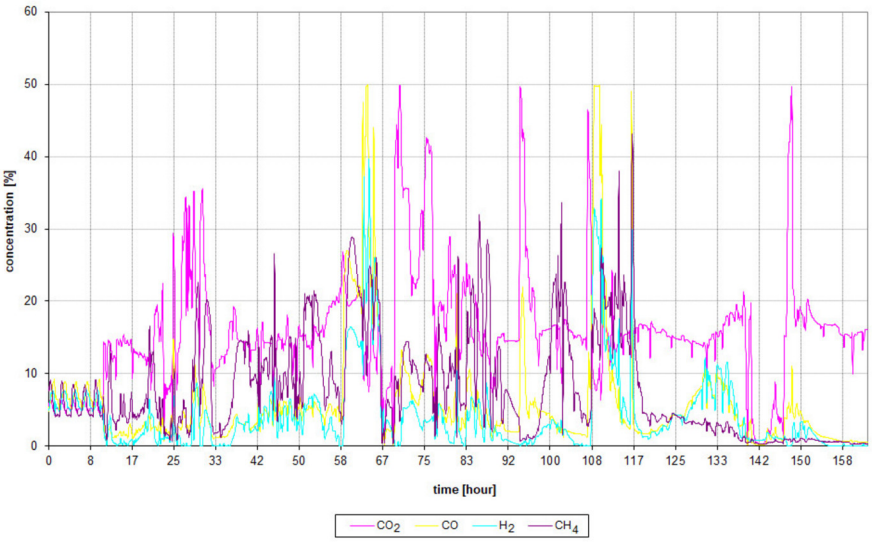

Figure 14. The syngas composition behavior during the first experiment.

Figure 15 shows the calorific value of the syngas during the first experiment. The highest calorific value of the syngas was measured approximately at the 117th hour of the experiment at 22.7 MJ/Nm^3. Relatively higher calorific values were recorded at the 58–67th hour of the experiment and at the 108–110th hour, at approx. 16.3 MJ/Nm^3. These periods corresponded to the part of the experiment where a mixture of air and oxygen was used as the input oxidizer. The average calorific value during the entire experiment was 4.01 MJ/Nm^3.

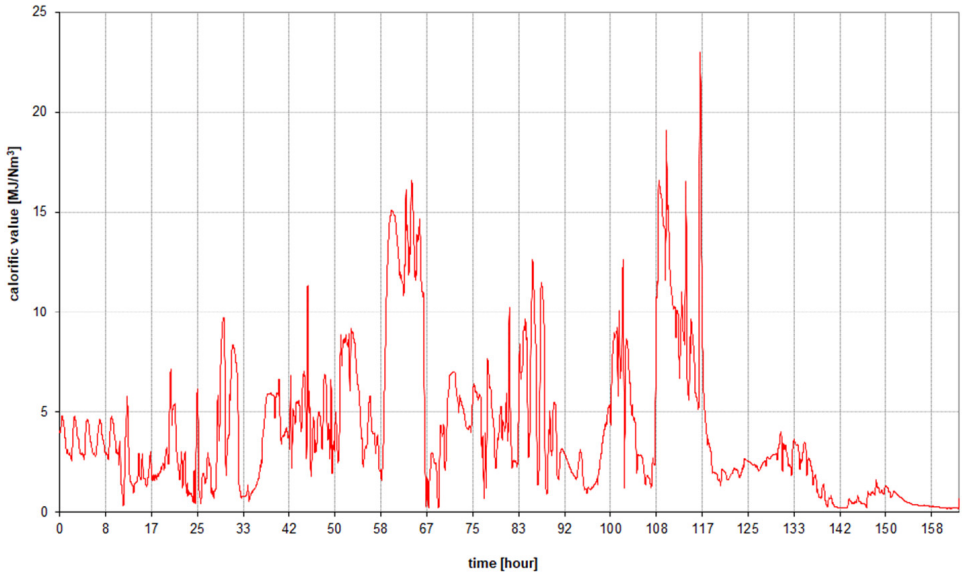

Figure 15. The calorific value of the syngas during the first experiment.

The course in the concentration of the heating components of the syngas in the second experiment is shown in Figure 16. The highest concentrations of the CO and H_2 components were measured in three periods during the gasification process, namely between the 27–28th hours, where the CO value was 49.7% and H_2 was 14.7%; between the 30th–31st hours, when the CO value was above 40% and H_2 was approx. 19%; and between the 52nd–53rd hours, where the value of CO was above 49.7% and H_2 was 15.8%. The highest calorific value of the syngas (Figure 17) was 11.6 MJ/Nm^3 and was measured during the 39–40th hour period. The average calorific value during the second experiment was 4.12 MJ/Nm^3.

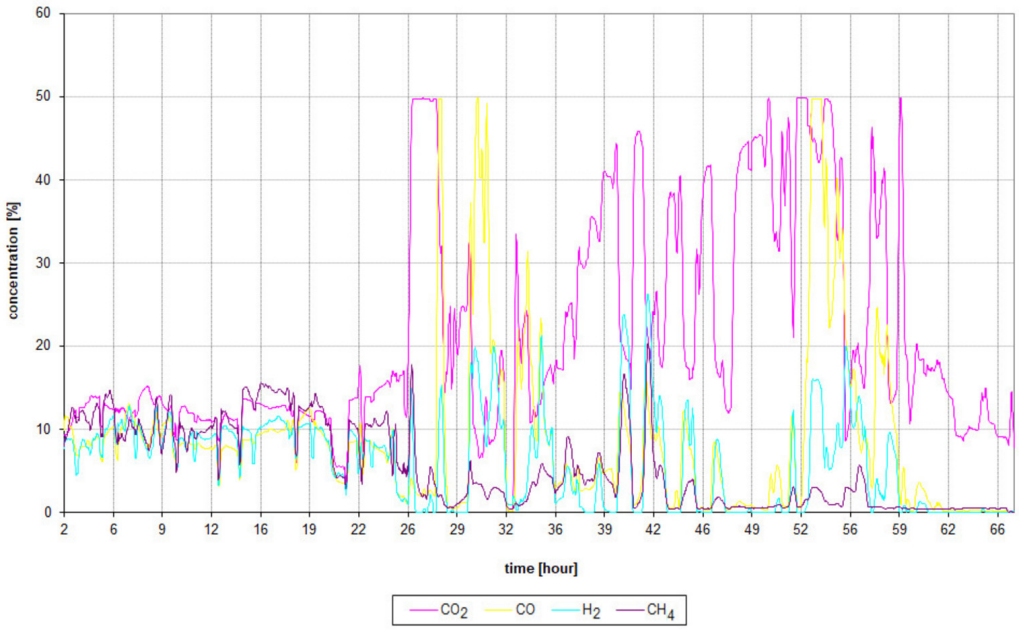

Figure 16. The syngas composition behavior during the second experiment.

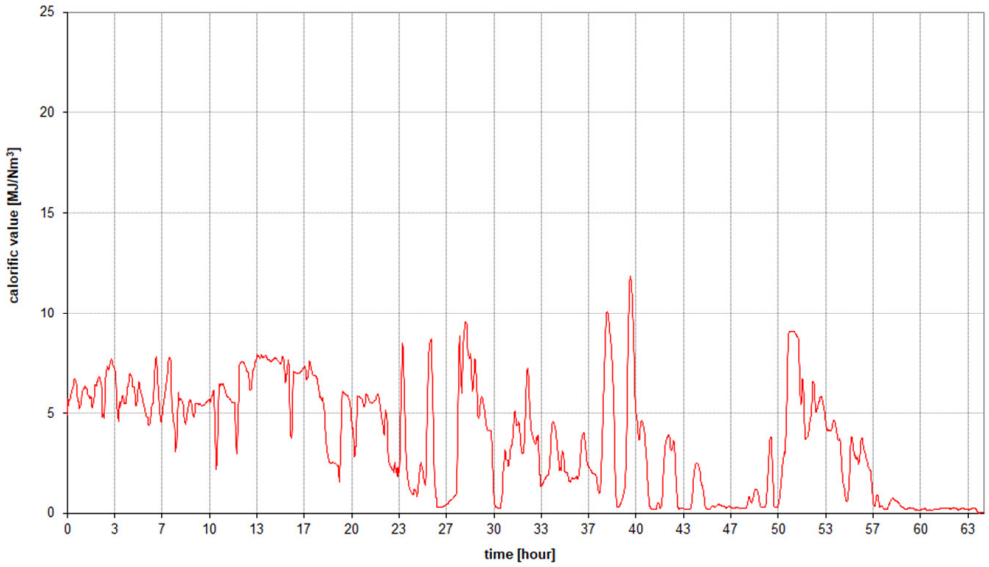

Figure 17. The calorific value of the syngas during the second experiment.

3.4. Results of the Model of Material Balance

The measured components, such as the flow of air, oxygen, and gas, their composition, and the mass of the condensate and coal, were used for the mass balance calculations. The calculated mass balance values for the first experiment are shown in Table 2, and the values for the second experiment are shown in Table 3. In addition, a loss component was determined as the difference between the inputs and outputs of the individual mass balance components. The loss component percentages in the individual experiments are shown in Figure 18a. The average loss percentage of the atoms (i.e., between the first and the second experiments) is shown in Figure 18b. The percentage of the atom losses obtained from the first experiment is shown in Figure 19a, and the percentage from the second experiment is shown in Figure 19b.

Table 2. The general and atomic balance values obtained from the first experiment calculations.

Balance	Input Materials (kg)			Output Materials (kg)				Losses
	Coal	Air	Oxygen	Unburned Coal	Ash	Gas	Condensate	
General	576	2221.49	5.74	75.5	80.22	2222.57	13.46	411.48
C	282.81	0	0	45.83	0	206.79	0	30.20
H	32.95	0	0	3.36	0	24.16	1.49	3.94
N	4.96	1703.86	0	0.80	0	1413.41	0	294.61
O	156.83	517.63	5.74	9.57	0	576.15	11.96	82.52
S	2.62	0	0	0.43	0	2.07	0	0.13

Table 3. The general and atomic balance values obtained from the second experiment calculations.

Balance	Input Materials (kg)			Output Materials (kg)				Losses
	Coal	Air	Oxygen	Unburned Coal	Ash	Gas	Condensate	
General	216	724.49	16.911	27	30.35	773.61	17.23	109.22
C	106.05	0	0	16.39	0	84.89	0	4.77
H	12.36	0	0	1.20	0	9.04	1.91	0.20
N	1.86	555.68	0	0.29	0	461.28	0	95.97
O	58.81	168.81	16.91	3.42	0	217.61	15.31	8.19
S	0.99	0	0	0.15	0	0.78	0	0.05

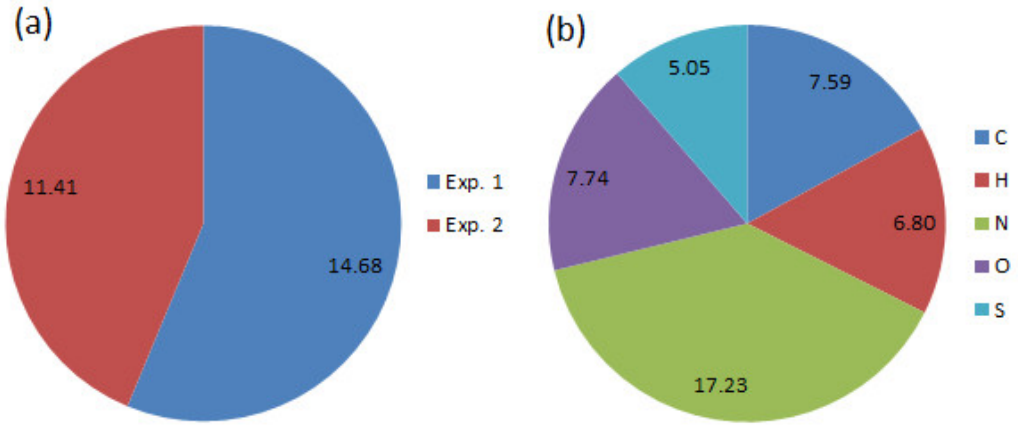

Figure 18. (**a**) Percentage of losses in the experiments; (**b**) average percentage of atom losses.

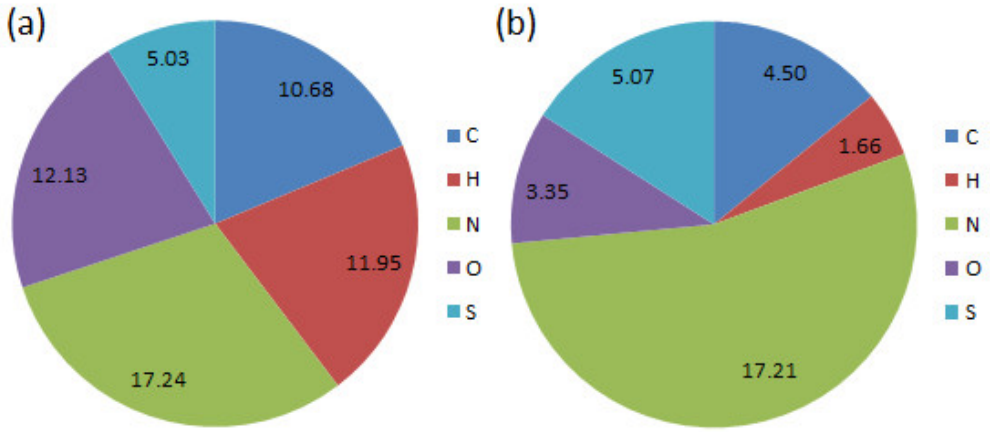

Figure 19. Percentage of atom losses; (**a**) the first experiment, (**b**) the second experiment.

The causes for the input and output materials difference were the air and oxygen leaks (i.e., atoms N and O) at the input side of the laboratory reactor and the produced gas leaks (i.e., atoms C, H, N, O, and S) at the output side of the laboratory reactor. The different perlite with a water glass layer between the experiments, i.e., the overburden in the first experiment and the overburden plus the left and right sides of the coal seam insulation in the second experiment, could be the cause of the higher losses in the first experiment. The perlite with a water glass layer formed a continuous impermeable layer in the initial stages of the experiment. Subsequently, its damage only occurred due to the effect of the increased temperature. The atoms O (i.e., 7.74%) and N (i.e., 17.23%) showed the highest losses during the atom loss average percentage calculation (Figure 18b). It follows that the most significant losses were on the pipeline at the input of the laboratory reactor. Figure 19 shows that the losses for element N were approximately the same, i.e., 17.24% and 17.21%. However, the losses for elements H, O, and C were significantly higher in the first experiment.

3.5. Results of the Effective Gasification Time

The effective gasification time was calculated for the condition of selecting the syngas with a minimum calorific value of 2.5 and 3 MJ/Nm^3. Tables 4 and 5 show the effective gasification time for setting the minimum calorific value condition of 2.5 and 3 MJ/Nm^3 in both experiments.

Table 4. The efficiency of the UCG process for the first experiment.

Cal. Val. Condition [MJ/Nm^3]	Effective Gasification Time [h]	Air Consum. [m^3]	O_2 Consum. [m^3]	Average Cal. Val. [MJ/Nm^3]	*ESR* [%]
>0	163.3	1935	29	4.01	
>2.5	93.7	1006	27	6.09	57.36
>3	77.5	737	26	6.78	47.48

Table 5. The efficiency of the UCG process for the second experiment.

Cal. Val. Condition [MJ/Nm^3]	Effective Gasification Time [h]	Air Consum. [m^3]	O_2 Consum. [m^3]	Average Cal. Val. [MJ/Nm^3]	*ESR* [%]
>0	64.5	340	38	4.12	
>2.5	37.3	204	15	5.81	57.89
>3	34.9	193	14	5.98	54.14

For the condition of a minimum calorific value of 2.5 MJ/Nm^3, the effective gasification time was 93.7 h, representing a 57.36% success rate in the first experiment. For the same condition of a minimum calorific value, the success rate in the second experiment was almost the same (57.89%). For the condition of a minimum calorific value of 3 MJ/Nm^3, the effective gasification time was 77.5 h (the first experiment) and 34.9 h (the second experiment), respectively, representing a 47.48% success rate (*ESR*) in the first experiment and 54.14% in the second experiment. From this point of view, the second experiment was more effective, despite the fact that the maximum calorific values were lower than in the first experiment. A higher *ESR* value means that a higher amount of heat energy is produced in the UCG process for the same minimum calorific value of the produced syngas. It was assumed that lower losses of the oxidizer to the surroundings of the ex-situ reactor caused a higher value for the effective gasification time. Subsequently, it caused a higher effect of the oxidizer on the gasification process. The higher amounts of the oxidizer (i.e., mainly air) in the first experiment were insufficient to support the gasification process due to the higher environmental losses to the environment. This fact reflects the permeability of the surrounding layers of the underground generator during the gasification in actual conditions.

In Tables 4 and 5, in addition to the effective gasification time, the air and oxygen consumption and the average calorific value for the given minimum calorific value are listed.

4. Conclusions

The paper described two experiments of the UCG process in laboratory conditions. The analyzed experiments were performed on two laboratory reactors. The experiments were analyzed regarding the achieved temperature and produced syngas composition and its calorific value. The second part of the paper analyzed the heat output of the produced gas using the material balance and efficiency of the UCG process.

The temperature was a significant variable for the UCG process. To create an oxidation zone, it was necessary to reach a temperature above 900 °C. The desired syngas was generated by the gasification reactions in the reduction zone at temperatures ranging from 550 to 900 °C. The maximal temperature in the gasification channel was around 1000 °C in both experiments. The highest calorific value of the syngas was measured at approximately 20 MJ/Nm^3 for the first experiment and 10 MJ/Nm^3 for the second experiment. These periods corresponded to the part of the experiment where a mixture of air and oxygen was used as the input oxidizer. Despite the difference in the maximal

values, the average calorific value was approx. the same in both experiments (i.e., the first experiment—4.01 MJ/Nm^3 and the second experiment—4.12 MJ/Nm^3).

The measured components, such as the flow of air, oxygen, and gas, their composition, and the mass of the condensate and coal, were used for the mass balance calculations. The causes of the difference between the input and output materials were the air and oxygen leaks (i.e., atoms N and O) at the input side of the ex-situ reactor and the produced gas leaks (i.e., atoms C, H, N, O, and S) at the output side of the ex-situ reactor. The percentage of losses in the first experiment was 14.68% and 11.41% in the second experiment. The experiment period was considered for the effective gasification time if the minimum value of the produced syngas was 2.5 and 3 MJ/Nm^3. The effective gasification time was better from the point of view of the achieved calorific value above 3 MJ/Nm^3 for the second experiment (i.e., 54.14%) than for the first experiment (i.e., 47.48%). Therefore, the second experiment was more efficient from the view of the material balance and effective gasification time.

Considering the achieved experimental results, it is possible to state the following.

- The calculation of the material balance during the gasification appears to be an effective tool for assessing the leaks from the reactor while measuring the flow and concentration of the oxidizers and produced gas.
- The material balance data make it possible to propose methods for controlling the input oxidizers (e.g., an increase in the oxidant flow in the event of its detected leakage before entering the oxidation zone).
- It is necessary to ensure the impermeable or poorly permeable surrounding layers of the coal seam to increase the efficiency of the gasification in an ex-situ reactor.
- The impermeability of the physical model will provide better conditions for controlling the UCG process.

In future research, it would be possible to design and implement methods for controlling the input oxidizing agents using a continuous evaluation of the material balance, and subsequently, assess the efficiency of the process in terms of the material and heat balance.

Author Contributions: Conceptualization, M.L. and M.D.; data curation, M.D.; formal analysis, P.F. and J.K.; methodology, M.D. and M.L.; software, M.L. and J.K.; project administration, M.L.; resources, M.D. and P.F.; supervision, M.L. and M.D.; validation, P.F. and J.K.; writing—original draft preparation, M.L. and M.D.; writing—review and editing M.D. and M.L.; All authors have read and agreed to the published version of the manuscript.

Funding: This research was funded by project COGAR RFCR-CT-2013-00002.

Data Availability Statement: No new data were created or analyzed in this study. Data sharing is not applicable to this article.

Acknowledgments: This work was supported by the Slovak Research and Development Agency under contract No. APVV-18-0526 and APVV-14-0892.

Conflicts of Interest: The authors declare no conflict of interest.

References

1. Yang, L.H.; Zhang, X.; Liu, S. Underground Coal Gasification Using Oxygen and Steam. *Energy Sources Part A Recovery Util. Environ. Eff.* **2009**, *31*, 1883–1892. [CrossRef]
2. Khan, M.; Mmbaga, J.; Shirazi, A.; Trivedi, J.; Liu, Q.; Gupta, R. Modelling Underground Coal Gasification—A Review. *Energies* **2015**, *8*, 2331. [CrossRef]
3. Stańczyk, K.; Kapusta, K.; Wiatowski, M.; Świądrowski, J.; Smoliński, A.; Rogut, J.; Kotyrba, A. Experimental simulation of hard coal underground gasification for hydrogen production. *Fuel* **2012**, *91*, 40–50. [CrossRef]
4. Gür, M.; Canbaz, E.D. Analysis of syngas production and reaction zones in hydrogen oriented underground coal gasification. *Fuel* **2020**, *269*, 117331. [CrossRef]
5. Feng, L.; Dong, M.; Wu, Y.; Gu, J. Comparison of Tar Samples from Reaction Zone and Outlet in Ex-Situ Underground Coal Gasification Experiment. *Energies* **2021**, *14*, 8570. [CrossRef]

6. Kapusta, K.; Wiatowski, M.; Stańczyk, K.; Zagorščak, R.; Thomas, H.R. Large-scale Experimental Investigations to Evaluate the Feasibility of Producing Methane-Rich Gas (SNG) through Underground Coal Gasification Process. Effect of Coal Rank and Gasification Pressure. *Energies* **2020**, *13*, 1334. [CrossRef]
7. Hamanaka, A.; Su, F.-Q.; Itakura, K.-I.; Takahashi, K.; Kodama, J.-I.; Deguchi, G. Experimental study on evaluation of underground coal gasification with a horizontal hole using two different coals. *Fuel* **2021**, *305*, 121556. [CrossRef]
8. Sadasivam, S.; Zagorščak, R.; Thomas, H.R.; Kapusta, K.; Stańczyk, K. Characterisation of inorganic constitutions of condensate and solid residue generated from small-scale ex situ experiments in the context of underground coal gasification. *Environ. Sci. Pollut. Res.* **2021**, *29*, 2203–2213. [CrossRef]
9. Su, F.-Q.; Zhang, T.; Wu, J.-B.; Deng, Q.-C.; Hamanaka, A.; Yu, Y.-H.; Dai, M.-J.; He, X.-L.; Yang, J.-N. Energy recovery evaluation and temperature field research of underground coal gasification under different oxygen concentrations. *Fuel* **2022**, *329*, 125389. [CrossRef]
10. Xiao, Y.; Yin, H.; Duan, T.; Qi, H.; Zhang, Y.; Jolfaei, A.; Xia, K. An Intelligent prediction model for UCG state based on dual-source LSTM. *Int. J. Mach. Learn. Cybern.* **2020**, *12*, 3169–3178. [CrossRef]
11. Lozynskyi, V.; Saik, P.; Petlovanyi, M.; Sai, K.; Malanchuk, Z.; Malanchuk, Y. Substantiation into Mass and Heat Balance for Underground Coal Gasification in Faulting Zones. *Inz. Miner. J. Pol. Miner. Eng. Soc.* **2018**, *20*, 289–300. [CrossRef]
12. Yang, L.; Zhang, X. Modeling of Contaminant Transport in Underground Coal Gasification. *Energy Fuels* **2008**, *23*, 193–201. [CrossRef]
13. Ekneligoda, T.C.; Yang, L.T.; Wanatowski, D.; Marshall, A.M.; Stace, L.R. Numerical Modelling of Ground Subsidence at an Underground Coal Gasification Site. *Geotech. Eng. J. SEAGS AGSSEA* **2017**, *48*, 151–154.
14. Falshtynskyi, V.; Saik, P.; Lozynskyi, V.; Dychkovskyi, R.; Petlovanyi, M. Innovative aspects of underground coal gasification technology in mine conditions. *Min. Miner. Depos.* **2018**, *12*, 68–75. [CrossRef]
15. Irum, Q.; Khan, S.A.; Uppal, A.A.; Krivodonova, L. Galerkin Finite Element Based Modeling of One Dimensional Packed Bed Reactor for Underground Coal Gasification (UCG) Process. *IEEE Access* **2020**, *8*, 223130–223139. [CrossRef]
16. Sawyer, W.K.; Shuck, L. Numerical Simulation of Mass and Energy Transfer in the Longwall Process of Underground Gasification of Coal. In *Society of Petroleum Engineers*; SPE Symposium on Numerical Simulation of Reservoir Performance: Los Angeles, CA, USA, 1976; p. 16. [CrossRef]
17. Lozynskyi, V.; Dichkovskiy, R.; Saik, P.; Falshtynskyi, V. Coal seam gasification in faulting zones (heat and mass balance study). *Solid State Phenom.* **2018**, *277*, 66–79. [CrossRef]
18. Bhutto, A.W.; Bazmi, A.A.; Zahedi, G. Underground coal gasification: From fundamentals to applications. *Prog. Energy Combust. Sci.* **2013**, *39*, 189–214. [CrossRef]
19. Saik, P.; Berdnyk, M. Mathematical model and methods for solving heat-transfer problem during underground coal gasification. *Min. Miner. Depos.* **2022**, *16*, 87–94. [CrossRef]
20. Krajňák, J.; Homišin, J.; Grega, R.; Kaššay, P.; Urbanský, M. The failures of flexible couplings due to self-heating by torsional vibrations—Validation on the heat generation in pneumatic flexible tuner of torsional vibrations. *Eng. Fail. Anal.* **2021**, *119*, 104977. [CrossRef]
21. Laciak, M.; Kostúr, K.; Durdán, M.; Kačur, J.; Flegner, P. The analysis of the underground coal gasification in experimental equipment. *Energy* **2016**, *114*, 332–343. [CrossRef]
22. Kostúr, K.; Sasvari, T.; Koštial, I.; Laciak, M.; Durdán, M.; Kačur, J.; Kuffa, S.; Mikula, J.; Ďurove, J.; Vavrek, P.; et al. *Underground Coal Gasification by Thermal Decomposition*; Research Report of Project APVV-0582-06; Technical University, Faculty BERG, ÚRaIVP: Kosice, Slovakia, 2008.
23. Balu, K.; Satyamurthi, N.; Ramalingam, S.; Deebika, B. *Problems on Material and Energy Balance Calculation*; I K International Publishing House: New Delhi, India, 2009.
24. Ghasem, N.; Henda, R. *Principles of Chemical Engineering Processes: Material and Energy Balances*, 2nd ed.; CRC Press: Boca Raton, FL, USA, 2014.